Scilight

Progress in Composite Materials
https://www.sciltp.com/journals/pcm

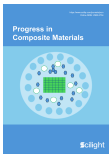

Article

Check for updates

Efficient Laser-Diode to Germanate-Tellurite Composite Fiber Excitation via Hyperbolic Microlens on Fiber-Tip

Anup Karak [1] and Sanchita Pramanik [2,*]

[1] Department of Physics, Centre for Distance and Online Education, Vidyasagar University, Midnapore 721102, West Bengal, India
[2] Department of Electronics, Vidyasagar University, Midnapore 721102, West Bengal, India
* Correspondence: pramanik_sanchita@yahoo.co.in

How To Cite: Karak, A.; Pramanik, S. Efficient Laser-Diode to Germanate-Tellurite Composite Fiber Excitation via Hyperbolic Microlens on Fiber-Tip. *Progress in Composite Materials* **2026**, *2*(1), 5. https://doi.org/10.53941/pcm.2026.100005

Received: 30 July 2026
Revised: 8 October 2026
Accepted: 23 November 2026
Published: 27 November 2026

Abstract: The optimized launch of laser light into an optical fiber is highly important in the field of fiber optics and photonics. In the present work, we investigate the coupling efficiency of a laser diode to the Germanate-Tellurite composite fiber with step and graded refractive index profiles via a hyperbolic microlens formed on the fiber tip. The laser beam propagation is analyzed applying the ABCD matrix formalism; meanwhile, the propagation characteristics of the composite fiber are obtained using the finite difference method. In the current work we numerically compute the fundamental modal field for the estimation of the coupling efficiency, which gives a more accurate calculation of the mode matching. We examine the impact of refractive-index profile, operating wavelengths, core radius, and focal length of the microlens on the coupling performance. The maximum coupling efficiency of about 98–99% is achieved in almost all the core radius values while varying the focal length of the microlens under ideal condition when misalignment is not considered. We also observe that the optimum focal lengths are increasing with the increasing values of core radii in both the step and graded refractive index profiles. We further estimate the coupling efficiency between the laser diode and Germanate-Tellurite composite fiber under both the transverse and angular misalignment conditions and observe that the coupling efficiency is significantly affected by small change in both misalignment values. The proposed approach prescribes the conditions for optimum launch of laser light in Germanate-Tellurite composite fibers and determines the suitability of hyperbolic microlenses for efficient excitation. This model can be readily extended to other soft-glass-based composite fibers which have various applications over the wide wavelength region in linear and nonlinear optics.

Keywords: composite optical fiber; spot size; lens coupling; microlens; finite difference method; ABCD matrix formalism

1. Introduction

Silica-based optical fibers have been dominating the optical fiber communication systems for few decades due to their established fabrication technology, low transmission loss, etc. [1–3]. However, their comparatively low nonlinear coefficient, fixed zero-dispersion characteristics, and limited infrared transmission window restrict the use of such fibers in many emerging photonic applications, mainly in near and mid-infrared wavelength regions. Subsequently, several works have shifted in the direction of soft-glass-based fibers such as chalcogenide [4], tellurite [5–7] etc., which provide relatively high nonlinearities, wider transmission windows, and improved flexibility in dispersion engineering [8,9]. In parallel, the composite materials are attracting extensive attention

Copyright: © 2026 by the authors. This is an open access article under the terms and conditions of the Creative Commons Attribution (CC BY) license (https://creativecommons.org/licenses/by/4.0/).
Publisher's Note: Scilight stays neutral with regard to jurisdictional claims in published maps and institutional affiliations.

due to the reason that an appropriate combination of the constituent materials will be able to offer superior performance in comparison to the separate components, which is enabling the improved functionality for essential technological and engineering applications [10].

The above idea has given rise to the progress of various composite soft-glass-based fibers in the optical fiber technology, where the different glass compositions are integrated to obtain controlled dispersion, improved optical confinement, extended infrared transmission, and nonlinear responses [11–14]. Among various composite materials, germanate-tellurite composite fibers (GTCFs) have recently received remarkable attention due to its admirable infrared transparency, high nonlinearity performance, and good mechanical stability and compatibility of germanate glass with the tellurite glass [13–15]. The combination of tellurite-glass (TWL) as the core and germanate-glass (GTZN) as the cladding gives the large refractive-index difference without creating any structural defects at the fiber interface. Such kinds of composite fibers exhibit high optical confinement and small effective areas, allowing the transmission to nearly 5.5 μm, empowering them for supercontinuum generation, Raman amplification, nonlinear wavelength conversion, and many other mid-infrared photonic applications [14,15]. In a recent work, we reported that by changing the core radius and choosing various refractive-index profiles (RIPs) in the GTCFs, the zero-dispersion region can be shifted and flattened over a wide spectral wavelength. It is also shown that keeping the favourable nonlinear properties, the triangular RIPs provide comparatively broader near-zero dispersion characteristics [15]. Many literatures have reported propagation dynamics like dispersion analysis, effective area, nonlinearity [15–17] etc. and various Raman gain properties with different types of fiber profiles and profile imperfections [18], loss estimations [19–22], efficient lensing schemes of conventional fibers, photonic crystal fibers and other specialty fibers [23–34]. In addition, extensive effort are also made to optimize the propagation dynamics of soft-glass based composite fibers [14,15], but, less attention is paid to the equally significant real problem, namely, the efficient launching of laser light into the various composite fibers. The coupling efficiency is directly involved with the usable optical power available inside the fiber in almost all experimental systems, and hence it immensely affects the performance of sensing systems and nonlinear devices.

The hyperbolic microlenses (HML) fabricated on the tip of the fibers have been established to give noticeably higher coupling efficiency compared to the conventional tapered [35–37] or Parabolic microlenses [38–41] since they minimize the spherical aberration while keeping admirable self-alignment characteristics. Furthermore, the study on characterizing and practical design of lens is carried out for the ease of these kinds of works [24,42–48]. Many investigations based on ABCD matrix formalism have been carried out for predicting laser-to-fiber coupling efficiencies in optical fibers like conventional circular-core fibers, photonic crystal fibers, and elliptic-core fibers [26–28,35,36]. However, these analyses predicted the fiber modal spot-size considering the analytical approximations or empirical relations and are usually suitable for silica-based fibers. In the case of high-index-contrast soft-glass composite fibers holding different RIPs, these approximations become less reliable [15].

The laser light-to-fiber coupling scheme has previously been investigated for silica based conventional fibers and photonic crystal fibers (PCFs) via HML [27,28,49]. In earlier work, HML-assisted coupling to silica-based PCFs was analyzed using the ABCD matrix method, with the modal spot size obtained employing an analytical approximation. In this work, we considered the coupling of laser light into GTCFs via a HML formed on the tip of the fiber where the fundamental mode for estimation of the coupling efficiency is numerically computed, which gives a more accurate calculation of the mode matching. These numerically estimated parameters are incorporated into the ABCD matrix formalism to accurately predict the coupling efficiency. The impact of various RIPs, operating wavelengths, core radius, and focal length of the microlens on the coupling performance are also investigated. In addition to this, the coupling efficiency due to various misalignments like transverse and angular mismatch between the laser diode and GTCF is also calculated.

The organization of this paper is as follow: Methodology is described in the Section 2, the Results and Discussion Section is described in the Section 3 and finally the Conclusions part is described in the Section 4.

2. Methodology

The proposed coupling scheme comprises of a laser diode, free-space region, an HML fabricated on the tip of the fiber and the GTCF. The entire configuration for computing the coupling efficiency is described in the following two sections:

2.1. Spot-Size Calculation of Composite Fiber

In this work, the RIPs of the fiber are defined as [15]:

$$n^2(r) = \begin{cases} n_{CO}^2 - (n_{CO}^2 - n_{Cl}^2)\left(\frac{r}{a_C}\right)^q; & 0 \le r \le a_C \\ n_{Cl}^2; & r > a_C \end{cases} \quad (1)$$

where, n_{CO}, n_{Cl} and a_C are, refractive index of core, refractive index of cladding and core radius of the fiber respectively. Also, $q = \infty$ for step RIP and $q = 1$ for triangular RIP and the radial distance, $r = \sqrt{x^2 + y^2}$.

The material combinations $69TeO_2 - 23WO_3 - 8LaO_3$ (TWL) and $47.5GeO_2 - 17.5TeO_2 - 20ZnO - 15Na_2O$ (GTZN) are considered respectively to design core and cladding regions of composite fiber and their wavelength dependent refractive indices are formulated using the Sellmeier equation as given below [14].

$$n^2 = A + \frac{B_1}{1 - \left(\frac{C_1}{\lambda^2}\right)} + \frac{B_2}{1 - \left(\frac{C_2}{\lambda^2}\right)} \quad (2)$$

where, the Sellmeier coefficients for TWL glass are $A = 2.225$, $B_1 = 2.009$, $B_2 = 1.475$, $C_1 = 0.04767\ \mu m^2$ and $C_2 = 149.2\ \mu m^2$ and that for GTZN glass are $A = 1.679$, $B_1 = 1.292$, $B_2 = 0.5$, $C_1 = 0.03045\ \mu m^2$ and $C_2 = 149.5\ \mu m^2$.

The combination of this core and cladding to form a composite fiber has formerly been experimentally adopted and the fiber is also fabricated and examined for applications in nonlinear optics. The same composite material based fiber with the choice of different refractive index profiles is investigated in our recent work. In the present work, the corresponding material parameters are considered from the available experimental literature for the efficient coupling of laser light on the GTCF.

Now, to evaluate the fundamental modal field of the GTCFs having various RIPs, we solve the Helmholtz equation which is given below for the electric field $\vec{E}(x, y, z)$ [15].

$$\nabla^2 \vec{E} + \vec{\nabla}\left(\frac{\vec{E}}{n^2}.\vec{\nabla}n^2\right) = k_0^2 n^2 \vec{E} \quad (3)$$

where, $k_0 = 2\pi/\lambda$.

Considering the circularly symmetric structure of the composite fiber used in the proposed lensing scheme, we have applied the semi-vectorial FDM which calculates the modal field and the effective refractive index of the GTCF fairly excellently with less effort. Furthermore, for a guided mode, the electric field $\vec{E}(x, y, z) = \vec{E}(x, y)e^{-j\beta z}$. Since there is no index variation along the *z*-direction, the *z*-dependent part is omitted. Only transverse components of $\vec{E}$ (E_x or E_y) will be coupled.

Now, the modal intensity involving the modal electric field $\vec{E}(x, y)$ may be calculated using the following equation

$$I(x, y) = \left|\vec{E}(x, y)\right|^2 \quad (4)$$

Again, the beam centroid coordinates, x_c and y_c of the numerically calculated modal intensity distribution, $I(x, y)$ are obtained with the help of first order intensity moment [50],

$$x_c = \frac{\iint x\, I(x, y)dxdy}{\iint I(x, y)dxdy} \quad (5)$$

$$y_c = \frac{\iint y\, I(x, y)dxdy}{\iint I(x, y)dxdy} \quad (6)$$

where, the denominator term in both Equations (5) and (6) represents the total power, and is defined as

$$P = \iint I(x, y)dxdy \quad (7)$$

Since, the chosen fiber is circularly symmetric, therefore $x_c = y_c = 0$

The modal spot sizes are calculated directly from the second moments [50,51] of the field obtained from the FDM and is written as,

$$w_x = 2\sqrt{\frac{\iint x^2\, I(x, y)dxdy}{\iint I(x, y)dxdy}} \quad (8)$$

$$w_y = 2\sqrt{\frac{\iint y^2 I(x,y)dxdy}{\iint I(x,y)dxdy}} \tag{9}$$

Now, the equivalent Gaussian modal fields constructed using the above two numerically obtained spot sizes is

$$E_G(x,y) = exp\left[-\left\{\frac{x^2}{w_x^2}+\frac{y^2}{w_y^2}\right\}\right] \tag{10}$$

This equivalent Gaussian modal field is constructed here for its use in simple and elegant optimization analytical formula. To obtain the closed-form coupling efficiency expression from the overlap-integral formula, the use of this equivalent Gaussian modal field is explained in the next section. Again, as our chosen fiber is circularly symmetric, the fiber spot size will be $w_x = w_y = w_f$.

2.2. Formulation for Lens Coupling

The proposed coupling configuration is shown in Figure 1. The focal length, in between the HML placed at the end face of the GTCF and the laser light source is defined by *f*. The intensity profile of the laser beams emitted from laser diode is considered to have spot sizes w_{1x} and w_{1y} alongside the two mutually perpendicular directions. Furthermore, we consider that the transmission loss is negligible, the laser source exhibits the Gaussian field distributions, and there is a perfect matching of the polarisation mode on the microlens surface and that of the fiber field. Additionally, an appropriate angular width of the microlens is selected to capture the whole power emitted by the laser source for the given set of microlens parameters. Again, to eliminate the spherical aberration the distance between the laser diode and adjacent point of the HML is set to the focal length of the microlens.

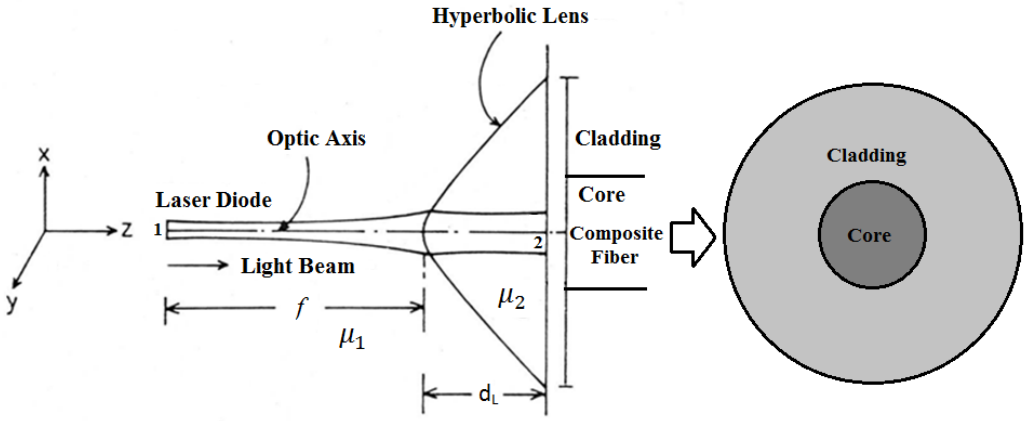

Figure 1. Geometry of the coupling scheme of laser diode to germanate-tellurite composite fiber (GTCF).

Now, the output field of the laser diode at a distance *u,* from the HML (shown in plane 1 of the Figure 1) can be expressed as:

$$E_L(x,y) = E_{0L} \cdot exp\left[-\left\{\frac{x^2}{w_{1x}^2}+\frac{y^2}{w_{1y}^2}\right\}\right] \tag{11}$$

where, $E_{0L} = exp\left[-\frac{ik_1}{2}\left\{\frac{x^2+y^2}{R_1}\right\}\right]$, w_{1x} and w_{1y} are the spot sizes of the laser light beams emitted from source laser along the two perpendicular directions, R_1 is the radius of curvature of the wave-fronts of laser source and k_1 is the incident medium's wave number. In this study, we considered the single frequency laser emitting one spatial mode with a Gaussian intensity profile.

Now the microlens transformed laser field on the fiber plane 2, shown in Figure 1 can be written as

$$E_T(x,y) = E_{0T} \cdot exp\left[-\left\{\frac{x^2}{w_{2x}^2}+\frac{y^2}{w_{2y}^2}\right\}\right] \tag{12}$$

where, $E_{0T} = exp\left[-\frac{ik_2}{2}\left\{\frac{x^2}{R_{2x}}+\frac{y^2}{R_{2y}}\right\}\right]$, w_{2x} and w_{2y} are microlens transformed spot sizes respectively, k_2 is microlens medium's wave number, and R_{2x} and R_{2y} are the transformed radii of curvature of the refracted wavefronts in the *X* and *Y* directions.

It is important to mention that, the microlens transformed spot sizes, w_{2x} and w_{2y} together with the transformed radii of curvature of the refracted wavefronts in the X and Y directions, R_{2x} and R_{2y} are estimated using the ABCD matrix formulation for an HML fabricated on the fiber tip. The necessary formulations involving w_{1x}, w_{1y} and R_1 are adopted from the previous reported work [28].

Finally, the laser source to GTCF coupling efficiency via HML on the tip of fiber can be written in terms of overlap integral as:

$$\eta = \frac{|\iint E_T(x,y)\cdot E_G^*(x,y)\,dxdy|^2}{\iint|E_T(x,y)|^2dxdy\cdot\iint|E(x,y)|^2dxdy} \tag{13}$$

This, analytical overlap integral equation is now evaluated applying the lens transformed laser light field and the equivalent Gaussian modal fields, $E_G(x,y)$. This $E_G(x,y)$ is constructed from numerically obtained spot sizes leading to the closed-form coupling efficiency expression in absence of any misalignment, for the GTCF and is written as [28].

$$\eta_m = \frac{4w_{2x}w_{2y}w_f^2}{\left[\left(w_f^2+w_{2x}^2\right)^2+\frac{k_2^2w_{2x}^4w_f^4}{4R_{2x}^2}\right]^{1/2}\left[\left(w_f^2+w_{2y}^2\right)^2+\frac{k_2^2w_{2y}^4w_f^4}{4R_{2y}^2}\right]^{1/2}} \tag{14}$$

Now, for a series of core radius values of the GTCF, having step and triangular RIPs in the core, the coupling efficiency with variation of the focal lengths are computed and the optimum focal length (f_0), for which the coupling efficiency is maximum, is determined. The investigation is carried out with two different wavelengths of practical interests, 1.3 μm and 1.5 μm.

Now in order to compute the coupling efficiency for the case of transverse misalignment in X-Y plane, we consider that the centre is shifted to (d_1,d_2) coordinates as shown in Figure 2. Therefore, the fundamental modal field in this misalignment condition will be calculated as:

$$E_G(x,y) = exp\left[-\left\{\frac{(x-d_1)^2}{w_x^2}+\frac{(y-d_2)^2}{w_y^2}\right\}\right] \tag{15}$$

Now, incorporating Equations (15) and (12) in the Equation (13), we get the transverse coupling efficiency (η_t) given as [50],

$$\eta_t = \eta_m\, exp\left[\frac{2d_1^2}{w_f^2}\left\{\frac{w_{2x}^2\left(w_f^2+w_{2x}^2\right)}{\left(w_f^2+w_{2x}^2\right)^2+\frac{k_2^2w_{2x}^4w_f^4}{4R_{2x}^2}}-1\right\}\right]\times exp\left[\frac{2d_2^2}{w_f^2}\left\{\frac{w_{2y}^2\left(w_f^2+w_{2y}^2\right)}{\left(w_f^2+w_{2y}^2\right)^2+\frac{k_2^2w_{2y}^4w_f^4}{4R_{2y}^2}}-1\right\}\right] \tag{16}$$

where, η_m is the coupling efficiency in absence of any misalignment whose value is given in Equation (14).

Again, we calculate the coupling efficiency for an angular mismatch, θ between the HML and GTCF as shown in the Figure 3. Therefore, the lens transformed field due to this angular misalignment can be addressed as,

$$E_T(x,y) = E_{0T}\cdot exp\left[-\left\{\frac{x'^2}{w_{2x}^2}+\frac{y'^2}{w_{2y}^2}\right\}\right] \tag{17}$$

here, $E_{0T} = exp\left[-\frac{ik_2}{2}\left\{\frac{x'^2}{R_{2x}}+\frac{y'^2}{R_{2y}}\right\}\right]$, and the fundamental modal field for GTCF under this angular misalignment is addressed as,

$$E_G(x,y) = exp\left[-\left\{\frac{x'^2+y'^2}{w_f^2}\right\}\right] \tag{18}$$

Now incorporating Equations (17) and (18) in Equation (13), we get the angular coupling efficiency (η_a) given as,

$$\eta_a = \eta_m\, exp\left[-\frac{k_2^2\theta^2}{2}\left\{\frac{w_{2x}^2w_f^2\left(w_f^2+w_{2x}^2\right)}{\left(w_f^2+w_{2x}^2\right)^2+\frac{k_2^2w_{2x}^4w_f^4}{4R_{2x}^2}}\right\}\right] \tag{19}$$

where, η_m is the coupling efficiency in absence of any misalignment whose value is given in Equation (14).

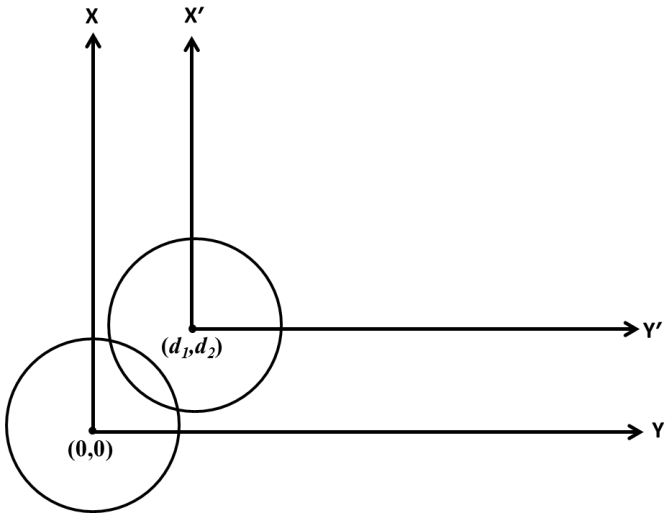

Figure 2. Transverse displacement between germanate-tellurite composite fiber (GTCF) centre and the image Laser spot.

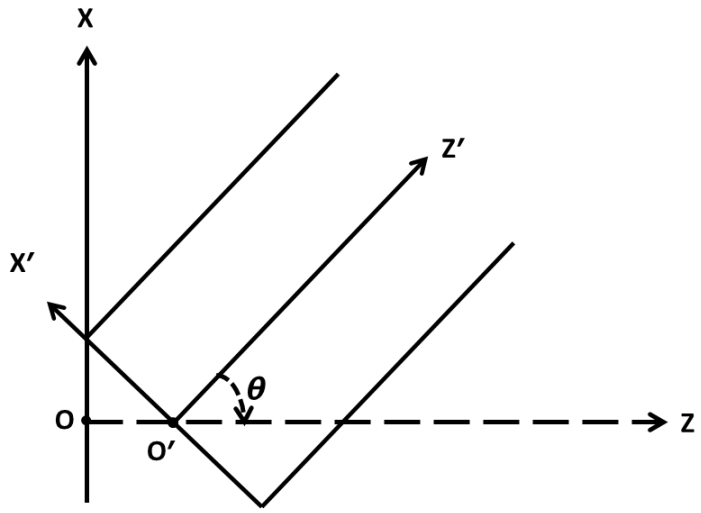

Figure 3. Angular displacement between germanate-tellurite composite fiber (GTCF) end face and the HML transformed input face and the image laser spot.

3. Results and Discussions

3.1. The Opto-Geometrical Parameters

To estimate the coupling efficiencies of GTCF via HML on the fibers tip, we considered two wavelengths of emitting light, one is 1.3 μm having the spot sizes w_{1x} = 1.081 μm and w_{1y} = 1.161 μm and another is 1.5 μm having spot sizes w_{1x} = 0.843 μm and w_{1y} = 0.857 μm [28]. The maximum microlens depth is defined by d_L = 6.0 μm. The refractive index of the material of the microlens (μ) is considered to be the index of the core material of the composite fiber. The choice of material is providing a platform of choosing practical wavelength dependent refractive index of lens material which is considered as constant value in the previous works [28]. Again, for simplicity, we have considered planar wave model for input beam from the laser facet.

3.2. Estimation of Coupling Efficiency of GTCF with Step RIP

The coupling efficiency between the laser diode to the GTCF with step RIP via HML on the fiber tip with variation of the focal length, for two different wavelengths 1.3 μm and 1.5 μm are calculated and shown in the Figures 4 and 5 respectively. The study is carried out for four different core radius values of this GTCF. From the figures, it is seen that the optimum focal length (f_0), for which the coupling efficiency is maximum, is increasing with increasing value of core radii. In the Table 1, we have presented the maximum coupling values and their corresponding optimum focal lengths of the GTCF with step RIP for four different values of the core radii. It is also

noticeable to mention that at the operating wavelength 1.3 μm, the gaps between two consecutive optimum focal lengths are comparatively high for two consecutive core radius values than that of operating wavelength 1.5 μm.

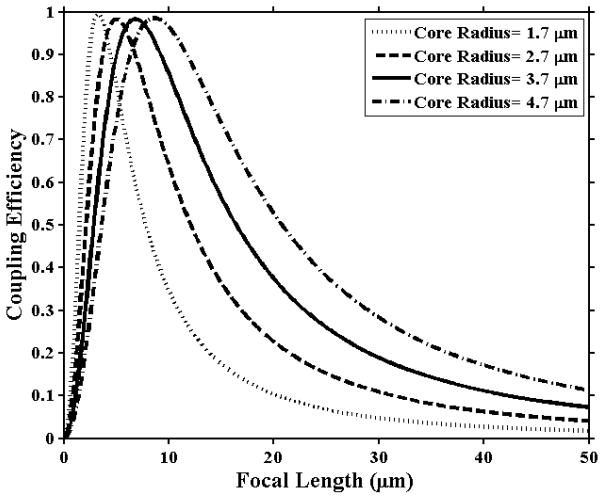

Figure 4. Coupling efficiency with change in focal length for GTCF with step RIP at 1.3 μm wavelength.

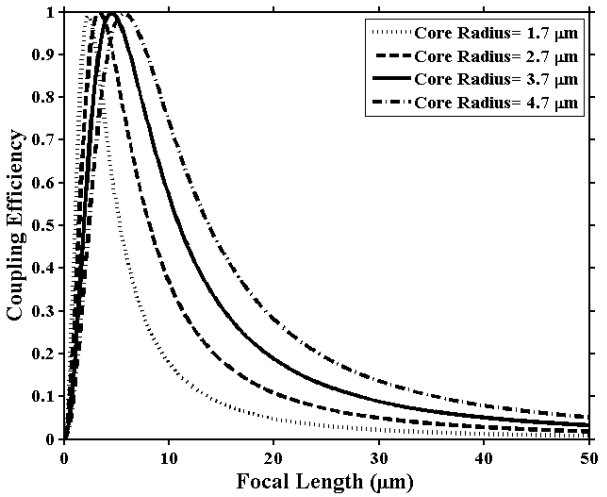

Figure 5. Coupling efficiency with change in focal length for GTCF with step RIP at 1.5 μm wavelength.

Table 1. The maximum coupling efficiency (η_m) at the corresponding optimum focal length (f_0) for different core radii for the two different operating wavelengths of practical interest in GTCF with step RIP.

Core Radii	Wavelength = 1.3 μm		Wavelength = 1.5 μm	
(μm)	f_0 (μm)	η_m	f_0 (μm)	η_m
1.7	3.3	0.995642	2.3	0.990826
2.7	5.0	0.983011	3.4	0.998881
3.7	6.8	0.982891	4.5	0.996324
4.7	8.6	0.985419	5.7	0.995739

3.3. Estimation of Coupling Efficiency of GTCF with Triangular RIP

Further, the coupling efficiency between the laser diode to the GTCF with triangular RIP via HML on the fiber tip with variation of the focal length, for two different wavelengths 1.3 μm and 1.5 μm are calculated and shown in the Figures 6 and 7 respectively. The study is carried out for four different core radius values for this fiber. From the figures, it is seen that the optimum focal length (f_0) for which the coupling efficiency is maximum, is increasing with increasing value of core radii. In the Table 2, we have presented the maximum coupling efficiency values and their corresponding optimum focal lengths for the GTCF with triangular RIP. Here also, we observe that at the operating wavelength 1.3 μm the gaps between the optimum focal lengths are comparatively high for two consecutive core radius values than that of operating wavelength 1.5 μm.

Here, with variation of core radii, the change in optimum focal length values for the GTCF with triangular RIP is lesser compared to the GTCF with step RIP.

Table 2. The maximum coupling efficiency (η_m) at the corresponding optimum focal length (f_0) for different core radii for the two operating wavelengths of practical interest in GTCF with triangular RIP.

Core Radii (μm)	Wavelength = 1.3 μm		Wavelength = 1.5 μm	
	f_0 (μm)	η_m	f_0 (μm)	η_m
1.7	2.3	0.939808	1.8	0.866062
2.7	2.5	0.980657	1.9	0.930485
3.7	2.6	0.993496	2.0	0.960754
4.7	2.8	0.997997	2.1	0.976728

For GTCFs with both the profiles, the maximum coupling efficiency are about 98–99%. The lensing scheme is much consistent in the triangular profile and the change in optimum focal length is also very less. Moreover, the optimum focal length values for achieving the maximum coupling efficiencies in the case of triangular RIPs are comparatively smaller than that of step RIPs at their corresponding core radius values. Therefore, the focal length is needed to be smaller in triangular RIPs of GTCF than the step RIPs of the GTCF.

Here, the calculated maximum coupling efficiency of about 98–99% is representing ideal modal overlap efficiency under the perfectly alignment and lossless interface conditions, but in practical case coupling efficiency will be lower due to presence of Fresnel reflection, surface imperfections, scattering, fabrication tolerances and thermal effects.

It is relevant to mention that, the roughness on the surface of the microlens is another source of loss through the scattering. It may add considerable impact on the scattering loss and reduce the coupling efficiency in practically fabricated devices. Since, the present analysis does not include any measured or specified surface-roughness data; its effect has not been considered for simplicity.

Furthermore, the current study focuses on optimizing the coupling efficiency between laser diode and GTCF via hyperbolic microlens and is based on a linear, room-temperature optical model. Thus, nonlinear effects of propagation, the thermal lensing, thermal expansion and thermo-optic effects are not incorporated in the present investigation. The coupling efficiency may be affected by nonlinear and thermal effects at the high optical power. Similarly, the continuous high-power operation, temperature-induced variations in microlens dimensions and refractive index may also modify the focal length and the condition of optimum coupling and hence the long-term stability of the coupling efficiency can be affected. In the future, these effects may be considered for further extension of the coupling scheme at high-power operation.

Again, the practical implementation of transverse displacement and angular deviation between laser and the fiber can reduce the modal overlap. Therefore, the coupling efficiency in the presence of transverse and angular misalignments is further elucidated and the corresponding results are illustrated in the following sections.

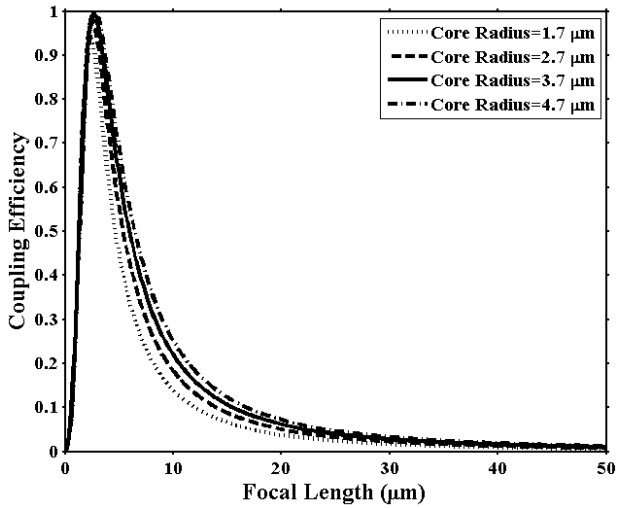

Figure 6. Coupling efficiency with change in focal length for GTCF with triangular RIP at 1.3 μm wavelength.

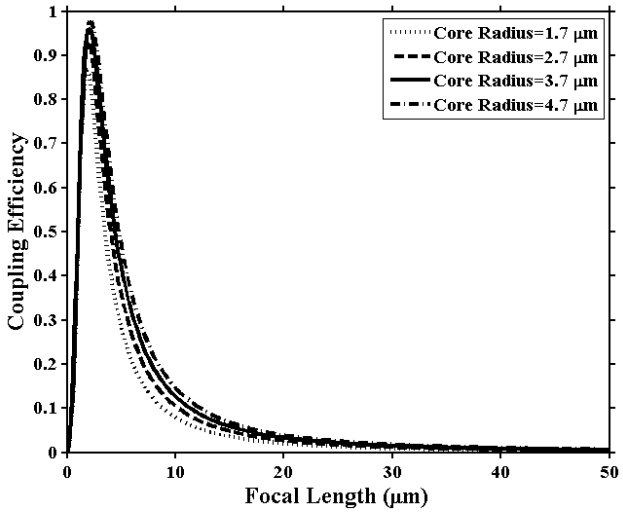

Figure 7. Coupling efficiency with change in focal length for GTCF with triangular RIP at 1.5 μm wavelength.

3.4. Estimation of Coupling Efficiency of GTCF with Step RIP in Presence of Misalignments

The coupling efficiency in the presence of transverse and angular misalignments for step RIP is computed for four different core radii values and tabulated in the Table 3. The η_{10} represents the coupling efficiency for the transverse misalignment due to shift of center by d_1 (=2 μm) along the *X*-axis where d_2 value is kept at zero. On the other hand, η_{01} is the coupling efficiency for the transverse misalignment due to shift of center by d_2 (=2 μm) along the *Y*-axis, where, d_1 value is kept at zero. Again, η_a represents the coupling efficiency due to angular misalignment and in the table we compute η_a keeping the angular misalignment value 3° [49].

Table 3. The transverse (η_{10} and η_{01}) and angular (η_a) coupling efficiency at the corresponding optimum focal length (f_0) for different core radii for the two different operating wavelengths of practical interest in GTCF with step RIP.

Core Radii (μm)	Wavelength = 1.3 μm				Wavelength = 1.5 μm			
	f_0 (μm)	η_{10}	η_{01}	η_a	f_0 (μm)	η_{10}	η_{01}	η_a
1.7	3.3	0.076358	0.063320	0.895032	2.3	0.086795	0.083299	0.911128
2.7	5.0	0.329677	0.305361	0.765253	3.4	0.335830	0.329798	0.827903
3.7	6.8	0.542202	0.519892	0.620689	4.5	0.541092	0.535745	0.712519
4.7	8.6	0.677753	0.659902	0.474665	5.7	0.678915	0.674673	0.583527

The variations of coupling efficiencies with the change of transverse misalignment between the centre of GTCF and the image laser spot for the step RIP GTCF are shown in Figures 8 and 9, where we see that the coupling efficiency is greatly affected by small change in the transverse mismatch in case of both the wavelengths 1.3 μm and 1.5 μm. Furthermore, the angular misalignment loss due to variation in the angular displacement between the GTCF end face and the HML transformed input face is computed and shown in the Figures 10 and 11 for both the wavelengths 1.3 μm and 1.5 μm. Here also, we see that the coupling efficiency is degrading with the increasing value of the angular misalignment. Moreover, we limit our investigations 0–2 μm and 0–3° in the case of transverse misalignment and angular misalignment respectively; since the system designers are generally interested with small values of the misalignments [49].

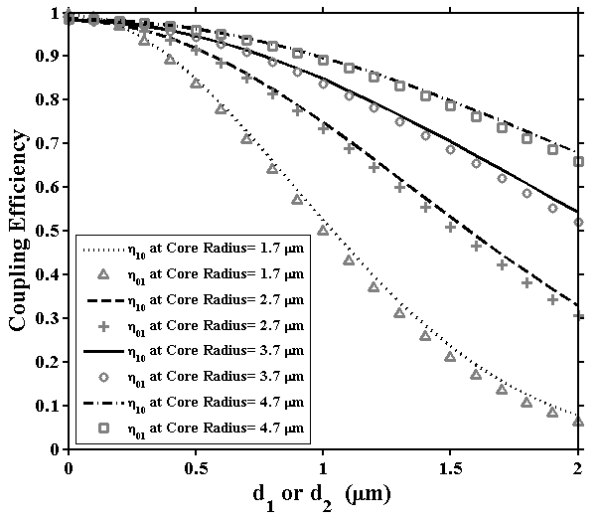

Figure 8. Coupling efficiency with change in transverse misalignment for GTCF with step RIP at 1.3 μm wavelength.

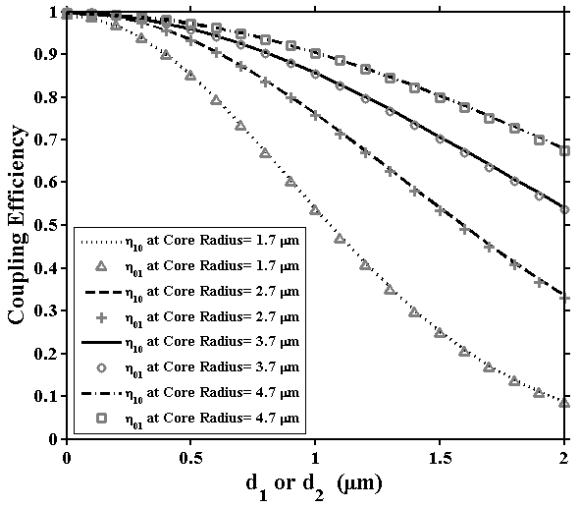

Figure 9. Coupling efficiency with change in transverse misalignment for GTCF with step RIP at 1.5 μm.

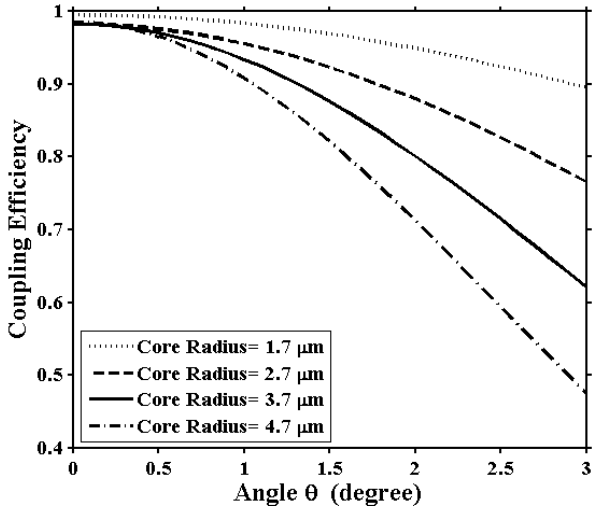

Figure 10. Coupling efficiency with change in angular misalignment for GTCF with step RIP at 1.3 μm.

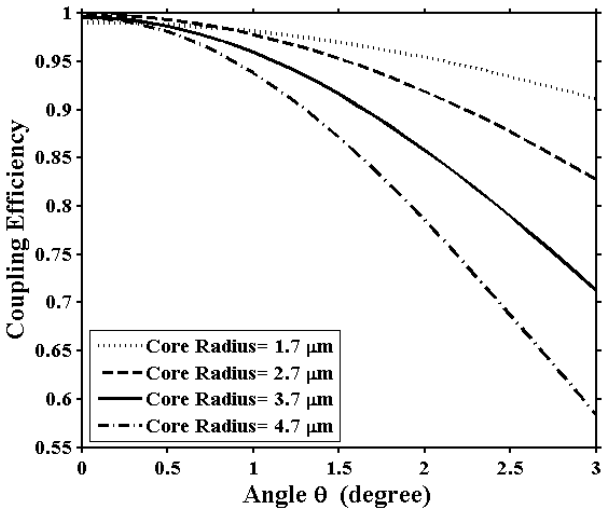

Figure 11. Coupling efficiency with change in angular misalignment for GTCF with step RIP at 1.5 μm.

3.5. Estimation of Coupling Efficiency of GTCF with Triangular RIP in Presence of Misalignments

Similarly, the coupling efficiencies for triangular RIP in the presence of transverse and angular misalignments is computed for four different core radii values and tabulated in the Table 4. Here also, for calculation of η_{10}, we considered d_1 = 2 μm along the *X*-axis at $d_2 = 0$; and for calculation of η_{01} we considered d_2 = 2 μm along the *Y*-axis, at $d_1 = 0$. For the calculation of η_a, we keep the angular misalignment value $\theta = 3°$.

Table 4. The transverse (η_{10} and η_{01}) and angular (η_a) coupling efficiency at the corresponding optimum focal length (f_0) for different core radii for the two different operating wavelengths of practical interest in GTCF with triangular RIP.

Core Radii (μm)	Wavelength = 1.3 μm				Wavelength = 1.5 μm			
	f_0 (μm)	η_{10}	η_{01}	η_a	f_0 (μm)	η_{10}	η_{01}	η_a
1.7	2.3	0.002594	0.001631	0.899003	1.8	0.011754	0.010946	0.829229
2.7	2.5	0.007752	0.005298	0.927590	1.9	0.022597	0.021235	0.882256
3.7	2.6	0.014158	0.010296	0.931748	2.0	0.036266	0.034331	0.903346
4.7	2.8	0.025482	0.019330	0.926409	2.1	0.052133	0.049642	0.911216

Further, the variations of coupling efficiencies with the variation of transverse misalignment between the centre of GTCF and the image laser spot for the triangular RIP GTCF are shown in Figures 12 and 13 at wavelengths 1.3 μm and 1.5 μm respectively. Here also, we see that the coupling efficiency is heavily affected by small change of the transverse mismatch. Again, the angular misalignment losses due to variation in the angular displacement between the GTCF end face and the HML transformed input face are calculated and shown in the Figures 14 and 15 for the wavelengths 1.3 μm and 1.5 μm.

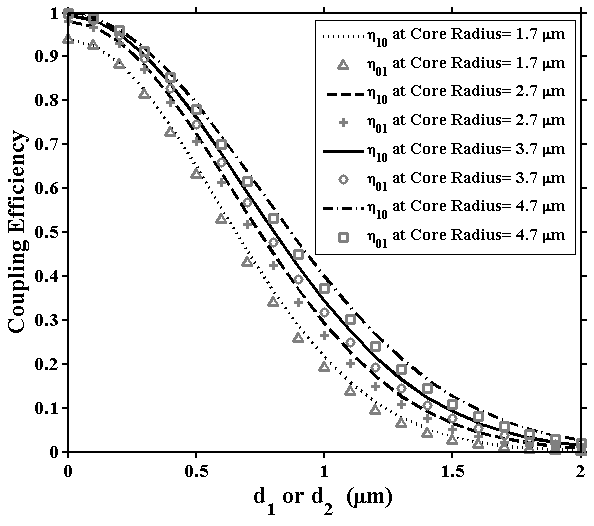

Figure 12. Coupling efficiency with change in transverse misalignment for GTCF with triangular RIP at 1.3 μm.

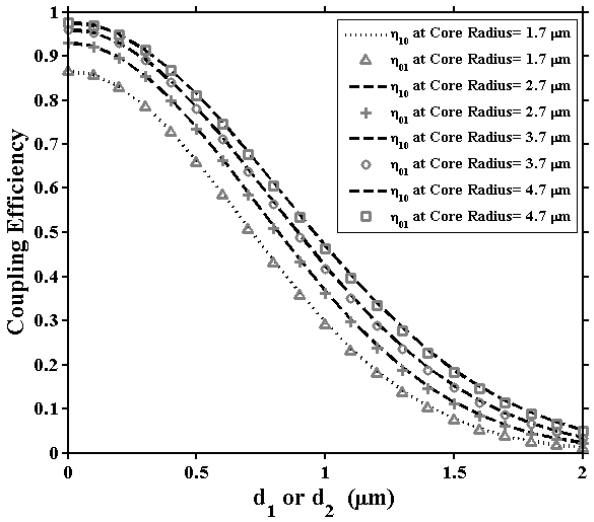

Figure 13. Coupling efficiency with change in transverse misalignment for GTCF with triangular RIP at 1.5 μm.

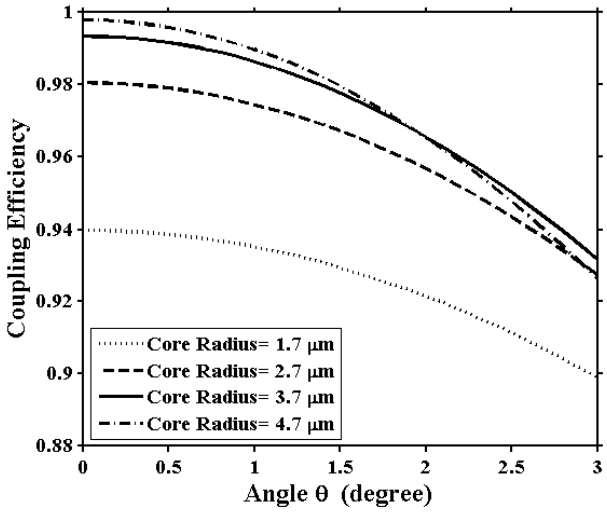

Figure 14. Coupling efficiency with change in angular misalignment for GTCF with triangular RIP at 1.3 μm.

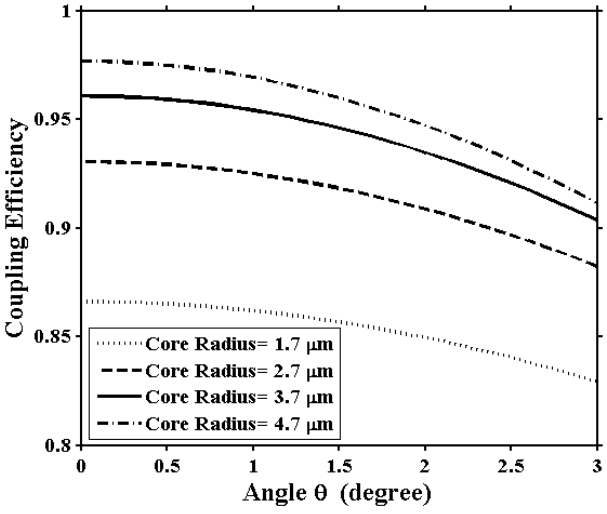

Figure 15. Coupling efficiency with change in angular misalignment for GTCF with triangular RIP at 1.5 μm.

Therefore, the proposed model of laser diode light coupling into GTCF via HML is beneficial for real implementation of such GTCFs for better coupling efficiency. Efficient coupling of laser light into these composite fibers can improve the performance of Raman amplifiers, wavelength converters, near and mid-infrared fiber lasers, supercontinuum sources, and broadband nonlinear devices etc. This approach can also be applied to the

other soft-glass fiber systems, including chalcogenide, fluoride, tellurite, germanate optical fibers and their composite combinations provided that the wavelength dependent refractive index is known. Since the various fiber parameters are achieved numerically through finite difference method, this recommended method gives a general framework for calculating maximum coupling efficiency and designing of the optimum launch of laser light for emerging soft-glass based optical fiber platforms.

4. Conclusions

We have investigated the coupling efficiency of a laser diode to the Germanate-Tellurite composite fiber via a hyperbolic microlens formed on the fiber tip for step and graded refractive index profiles of the composite fiber. The simple and analytical ABCD matrix formalism is applied here. Unlike earlier works that employed analytical approximations, in this work, we have numerically calculated the fundamental modal field and the corresponding spot-sizes of the composite fiber using the finite difference method and then estimate the coupling efficiency, which gives a more accurate calculation of the mode matching. The impact of refractive-index profile, operating wavelengths, core radius, and focal length of the microlens on the coupling performance is studied and the maximum coupling efficiency of about 98–99% is achieved considering the lossless interface conditions and ideal modal overlap due to perfectly alignment of laser diode and the GTCF in almost all the core radius values while varying the focal length of the microlens. We have also observed that the optimum focal lengths are increasing with the increasing value of core radii in both the step and triangular RIPs. Further, considering both the transverse and angular misalignment conditions, the coupling efficiency between the laser diode and GTCF is calculated and it is observed that, the coupling efficiency is significantly affected by small change in both the misalignment values. This study for calculating maximum coupling efficiency and its corresponding optimum focal length, will contribute immensely for the system designers and experimentalists during the launching of practical laser light into the composite fibers.

Author Contributions

A.K.: Conceptualization, methodology, data curation, writing—original draft preparation, visualization, investigation, supervision, validation, writing—reviewing and editing; S.P.: Conceptualization, methodology, data curation, writing—original draft preparation, visualization, investigation, supervision, validation, writing—reviewing and editing. All authors have read and agreed to the published version of the manuscript.

Funding

This research received no external funding.

Institutional Review Board Statement

Not applicable.

Informed Consent Statement

Not applicable.

Data Availability Statement

All data are available in the article.

Acknowledgments

The authors are grateful to the anonymous reviewers for their constructive and insightful suggestions.

Conflicts of Interest

The authors declare no conflict of interest.

Use of AI and AI-Assisted Technologies

No AI tools were utilized for this paper.

References

1. Snyder, A.W.; Love, J.D. *Optical Waveguide Theory*; Chapman and Hall: London, UK, 1983.
2. Ghatak, A.; Thyagarajan, K. *Introduction to Fiber Optics*; Cambridge University Press: Cambridge, UK, 1998. https://doi.org/10.1017/cbo9781139174770.
3. Marcuse, D. Loss Analysis of Single-Mode Fiber Splices. *Bell Syst. Tech. J.* **1977**, *56*, 703–718. https://doi.org/10.1002/j.1538-7305.1977.tb00534.x.
4. Samanta, C.; Karak, A.; Pramanik, S. Dispersion-Compensating Chalcogenide Coaxial Fiber: A Numerical Study. In Proceedings of the Second International Conference on Current Trends in Physics and Photonics (ICCTPP 2024), Pune, India, 9–11 July 2024; Vol. 13276. https://doi.org/10.1117/12.3044528.
5. Murugan, G.S.; Suzuki, T.; Ohishi, Y. Tellurite glasses for ultrabroadband fiber Raman amplifiers. *Appl. Phys. Lett.* **2005**, *86*, 161109. https://doi.org/10.1063/1.1906323.
6. Lin, A.; Zhang, A.; Bushong, E.J.; et al. Solid-core tellurite glass fiber for infrared and nonlinear applications. *Opt. Express* **2009**, *17*, 16716–16721. https://doi.org/10.1364/oe.17.016716.
7. Evrard, M.; Serrano, E.; Strutynski, C.; et al. (INVITED) Dispersion-shifted tellurite fibers for nonlinear frequency conversion. *Opt. Mater. X* **2022**, *15*, 100183. https://doi.org/10.1016/j.omx.2022.100183.
8. Marisova, M.P.; Andrianov, A.V.; Anashkina, E.A. Comprehensive Numerical Analysis of Temperature Sensitivity of Spherical Microresonators Based on Silica and Soft Glasses. *Sensors* **2023**, *23*, 717. https://doi.org/10.3390/s23020717.
9. Pniewski, J.; Stefaniuk, T.; Van, H.L.; et al. Dispersion engineering in nonlinear soft glass photonic crystal fibers infiltrated with liquids. *Appl. Opt.* **2016**, *55*, 5033–5040. https://doi.org/10.1364/ao.55.005033.
10. Gupta, M. Progress in Composite Materials. *Prog. Compos. Mater.* **2024**, *1*, 1. https://doi.org/10.53941/pcm.2025.100001.
11. Ahmadian, A.; Monfared, Y.E. Chalcogenide–Tellurite Composite Photonic Crystal Fiber: Extreme Non-Linearity Meets Large Birefringence. *Appl. Sci.* **2019**, *9*, 4445. https://doi.org/10.3390/app9204445.
12. Duan, Z.; Liao, M.; Yan, X.; et al. Tellurite Composite Microstructured Optical Fibers with Tailored Chromatic Dispersion for Nonlinear Applications. *Appl. Phys. Express* **2011**, *4*, 072502. https://doi.org/10.1143/apex.4.072502.
13. Boivin, M.; El-Amraoui, M.; Ledemi, Y.; et al. Thermal stress analysis and supercontinuum generation in germanate-tellurite composite fibers. *Opt. Mater. Express* **2016**, *6*, 1653–1662. https://doi.org/10.1364/ome.6.001653.
14. Boivin, M.; El-Amraoui, M.; Ledemi, Y.; et al. Germanate-tellurite composite fibers with a high-contrast step-index design for nonlinear applications. *Opt. Mater. Express* **2014**, *4*, 1740–1746. https://doi.org/10.1364/ome.4.001740.
15. Karak, A.; Samanta, C.; Pramanik, S. Effect of core radius on ZDW for Germanate-Tellurite composite fibers in the near and mid infrared regions. *Opt. Commun.* **2026**, *608*, 133061. https://doi.org/10.1016/j.optcom.2026.133061.
16. Russell, P.S.J. Photonic-Crystal Fibers. *J. Light. Technol.* **2006**, *24*, 4729–4749. https://doi.org/10.1109/jlt.2006.885258.
17. Karak, A.; Pramanik, S. Analysis and Dispersion Engineering for Generation of Ultra-flattened Dispersion in Photonic Crystal Fibers. In *Advances in Computer, Communication and Control*; Springer Singapore: Singapore, 2019; pp. 185–195. https://doi.org/10.1007/978-981-13-3122-0_18.
18. Pramanik, S.; Sarkar, S. Effect of dip in refractive index profile on fiber Raman gain amplifier performance. *Opt. Commun.* **2014**, *329*, 145–150. https://doi.org/10.1016/j.optcom.2014.05.016.
19. Karak, A.; Kundu, D.; Sarkar, S.N. Simplified Loss Estimation of Splice to Photonic Crystal Fiber using New Model. *J. Opt. Commun.* **2016**, *37*, 169–175. https://doi.org/10.1515/joc-2015-0043.
20. Xu, Z.; Duan, K.; Liu, Z.; et al. Numerical analyses of splice losses of photonic crystal fibers. *Opt. Commun.* **2009**, *282*, 4527–4531. https://doi.org/10.1016/j.optcom.2009.08.026.
21. Kundu, D. Estimation of splice losses between a photonic crystal fiber and a conventional single mode fiber and between two different photonic crystal fibers without and with transverse offset and angular misalignment. *J. Opt.* **2026**, *55*, 1470–1483. https://doi.org/10.1007/s12596-024-02194-1.
22. Karak, A.; Pramanik, S. Splice-Loss in Liquid-Filled Photonic Crystal Fibers. In Proceedings of the Second International Conference on Current Trends in Physics and Photonics (ICCTPP 2024), Pune, India, 9–11 July 2024; Vol. 13276. https://doi.org/10.1117/12.3044529.
23. Presby, H.M.; Edwards, C.A. Efficient coupling of polarization-maintaining fiber to laser diodes. *IEEE Photon. Technol. Lett.* **1992**, *4*, 897–899. https://doi.org/10.1109/68.149901.
24. Edwards, C.A.; Presby, H.M.; Dragone, C. Ideal microlenses for laser to fiber coupling. *J. Light. Technol.* **1993**, *11*, 252–257. https://doi.org/10.1109/50.212535.
25. John, J.; Maclean, T.S.M.; Ghafouri-Shiraz, H.; et al. Matching of single-mode fibre to laser diode by microlenses at 1.5 μm wavelength. *IEE Proc. Optoelectron.* **1994**, *141*, 178–184. https://doi.org/10.1049/ip-opt:19941052.
26. Gangopadhyay, S.; Sarkar, S. ABCD matrix for reflection and refraction of Gaussian light beams at surfaces of hyperboloid of revolution and efficiency computation for laser diode to single-mode fiber coupling by way of a hyperbolic lens on the fiber tip. *Appl. Opt.* **1997**, *36*, 8582–8586. https://doi.org/10.1364/ao.36.008582.

27. Mukhopadhyay, S.; Sarkar, S.N. Coupling of a laser diode to single mode circular core graded index fiber via hyperbolic microlens on the fiber tip and identification of the suitable refractive index profile with consideration for possible misalignments. *Opt. Eng.* **2011**, *50*, 045004(1–9). https://doi.org/10.1117/1.3570316.
28. Karak, A.; Kundu, D.; Mukhopadhyay, S.; et al. Investigation of coupling of a laser diode to photonic crystal fiber via hyperbolic microlens on the fiber tip by ABCD matrix formalism. *Opt. Eng.* **2015**, *54*, 086102. https://doi.org/10.1117/1.oe.54.8.086102.
29. Piccirillo, F.; Giaquinto, M.; Ricciardi, A.; et al. (INVITED) Miniaturized lenses integrated on optical fibers: Towards a new milestone along the lab-on-fiber technology roadmap. *Results Opt.* **2022**, *6*, 100203. https://doi.org/10.1016/j.rio.2021.100203.
30. Chen, Y.; Wang, C.; Xiao, L. Ultrathin Lensed Photonic Crystal Fibers with Wide Bandwidth and Long Working Distances. *J. Light. Technol.* **2021**, *39*, 2482–2488. https://doi.org/10.1109/jlt.2021.3050726.
31. Zandueta, J.; Lobo, S.; Saliou, F.; et al. Coupling light from laser to NANF with a hyperbolic profile fiber microlens. *Opt. Express* **2026**, *34*, 16179–16192. https://doi.org/10.1364/oe.587550.
32. Binti Kamarudin, S.N.H.; Lee, H.; Ishak, I.; et al. Rapid Direct Continuous Method for Hot Embossing of Glass Microlens Array Combined with CO_2 Laser Irradiation and External Preheating/Cooling. In *Recent Trends in Manufacturing and Materials towards Industry 4.0: Selected Articles from iM3F 2020, Malaysia*; Springer: Singapore, 2021; pp. 669–675. https://doi.org/10.1007/978-981-15-9505-9_60.
33. Peng, Z.S.; Wang, L. Optical Coupling between a Lensed Photonic Crystal Fiber and a Laser Diode. In Proceedings of the 2006 International Conference on Communications, Circuits and Systems, Guilin, Guangzi, China, 25–28 June 2006; Vol. 3, pp. 2005–2008. https://doi.org/10.1109/icccas.2006.285070.
34. Xiao, Y.; Chen, Y.; Liu, J.; et al. A monolithic microlens for an ytterbium-doped microstructured optical fiber amplifier. *Laser Phys.* **2019**, *29*, 035104. https://doi.org/10.1088/1555-6611/aaffc6.
35. Mondal, S.K.; Gangopadhyay, S.; Sarkar, S. Analysis of an upside-down taper lens end from a single-mode step-index fiber. *Appl. Opt.* **1998**, *37*, 1006–1009. https://doi.org/10.1364/ao.37.001006.
36. Yuan, L.B.; Shou, R.L. Formation and power distribution properties of an upside down taper lens at the end of an optical fiber. *Sens. Actuators A Phys.* **1990**, *23*, 1158–1161. https://doi.org/10.1016/0924-4247(90)87108-u.
37. Yuan, L.; Qui, A. Analysis of a single-mode fiber with taper lens end. *J. Opt. Soc. Am. A* **1992**, *9*, 950–952. https://doi.org/10.1364/josaa.9.000950.
38. Liu, H. The approximate ABCD matrix for a parabolic lens of revolution and its application in calculating the coupling efficiency. *Optik* **2008**, *119*, 666–670. https://doi.org/10.1016/j.ijleo.2007.01.014.
39. Liu, H.; Liu, L.; Xu, R.; et al. ABCD matrix for reflection and refraction of Gaussian beams at the surface of a parabola of revolution. *Appl. Opt.* **2005**, *44*, 4809–4813. https://doi.org/10.1364/ao.44.004809.
40. Mukhopadhyay, S. Efficient coupling of a laser diode to a parabolic microlens tipped circular core photonic crystal fiber using ABCD matrix formalism with consideration for possible misalignments. *J. Opt.* **2018**, *47*, 47–60. https://doi.org/10.1007/s12596-017-0443-9.
41. Bouhafs, Z.; Guessoum, A.; Guermat, A.; et al. Parabolic microlensed optical fiber for coupling efficiency improvement in single mode fiber. *Opt. Contin.* **2022**, *1*, 1218–1231. https://doi.org/10.1364/optcon.441633.
42. Song, J.H.; Fernando, H.N.J.; Roycroft, B.J.; et al. Practical Design of Lensed Fibers for Semiconductor Laser Packaging Using Laser Welding Technique. *J. Light. Technol.* **2009**, *27*, 1533–1539. https://doi.org/10.1109/jlt.2009.2014252.
43. Li, E. Characterization of a fiber lens. *Opt. Lett.* **2006**, *31*, 169–171. https://doi.org/10.1364/ol.31.000169.
44. Wen, C.; Hu, J.; Xu, W.; et al. A simple and low-cost fabrication method of microlens on optical fiber end facet. *Optik* **2020**, *214*, 164829. https://doi.org/10.1016/j.ijleo.2020.164829.
45. Matczak, S.; Stachowiak, D.; Soboń, G. Design and Fabrication of Fiber Optic Microlenses Using an Arc Fusion Splicing System. *J. Light. Technol.* **2025**, *43*, 6862–6872. https://doi.org/10.1109/jlt.2025.3563232.
46. Xiao, Y.; Zhou, G.; Xian, W.; et al. Fabrication of microlenses on ytterbium-doped double-cladding microstructured optical fibers with a CO_2 laser for effective optical coupling. *J. Opt.* **2019**, *48*, 123–128. https://doi.org/10.1007/s12596-018-0509-3.
47. Liu, M.; Zhang, F.; Xu, C.; et al. Coupling efficiency of laser diode to GRIN fiber by aspherical lens. *Opt. Fiber Technol.* **2022**, *73*, 103069. https://doi.org/10.1016/j.yofte.2022.103069.
48. Lu, S.; Zhang, F.; Xu, C.; et al. Coupling efficiency of a laser diode to a single-mode fiber via a microlens on the fiber tip. *Opt. Fiber Technol.* **2022**, *68*, 102766. https://doi.org/10.1016/j.yofte.2021.102766.
49. Karak, A.; Kundu, D.; Sarkar, S.N. Optimum Launch Optics Involving Laser Excited Photonic Crystal Fibers via Hyperbolic Microlens on Its Tip in Presence of Transverse and Angular Misalignments. In Proceedings of the 6th International Conference on Computers and Devices for Communication (CODEC), Kolkata, India, 16–18 December 2015.

50. International Organization for Standardization. *ISO 11146-1:2021*; Lasers and Laser-Related Equipment—Test Methods for Laser Beam Widths, Divergence Angles and Beam Propagation Ratios—Part 1: Stigmatic and Simple Astigmatic Beams; ISO: Geneva, Switzerland, 2021.
51. Siegman, A.E. How to (Maybe) Measure Laser Beam Quality. In Proceedings of the Diode Pumped Solid State Lasers: Applications and Issues, Bellingham, WA, USA, 27–28 January 1998. https://doi.org/10.1364/dlai.1998.mq1.